ACS OMEGA

http://pubs.acs.org/journal/acsodf

Article

Facile Electrochemical Demethylation of 2-Methoxyphenol to Surface-Confined Catechol on the MWCNT and Its Efficient Electrocatalytic Hydrazine Oxidation and Sensing Applications

Mansi Gandhi, Desikan Rajagopal,* and Annamalai Senthil Kumar*

Cite This: *ACS Omega* 2020, 5, 16208−16219

Read Online

ACCESS | Metrics & More | Article Recommendations | Supporting Information

ABSTRACT: Owing to its biological significance, preparation of stable surface-confined catechol (CA) is a long-standing interest in electrochemistry and surface chemistry. In this connection, various chemical approaches such as covalent immobilization (using amine- and carboxylate-functionalized CA, diazotization-based coupling, and Michael addition reaction), self-assembled monolayer on gold (thiol-functionalized CA is assembled on the gold surface), CA adsorption on the ad-layer of a defect-free single-crystal Pt surface, $\pi-\pi$ bonding, CA pendant metal complexes, and CA-functionalized polymer-modified electrodes have been reported in the literature. In general, these conventional methods are involved with a series of time-consuming synthetic procedures. Indeed, the preparation of a surface-fouling-free surface-confined system is a challenging task. Herein, we introduce a new and facile approach based on electrochemical demethylation of 2-methoxyphenol as a precursor on the graphitic surface (MWCNT) at a bias potential, 0.5 V vs Ag/AgCl in neutral pH solution. Such an electrochemical performance resulted in the development of a stable and well-defined redox peak at $E^{o'}$ = 0.15 (A2/C2) V vs Ag/AgCl within 10 min of preparation time in pH 7 phosphate buffer solution. Calculated surface excess (16.65×10^{-9} mol cm^{-2}) is about 10−1000 times higher than the values reported with other preparation methods. The product (catechol) formed on the modified electrode was confirmed by collective electrochemical and physicochemical characterizations such as potential segment analysis, TEM, Raman, IR, UV−vis, GC−MS, and NMR spectroscopic techniques, and thin-layer chromatographic studies. The electrocatalytic efficiency of the surface-confined CA system was demonstrated by studying hydrazine oxidation and sensing reactions in a neutral pH solution. This new system is found to be tolerant to various interfering biochemicals such as uric acid, xanthine, hypoxanthine, glucose, nitrate, hydrogen peroxide, ascorbic acid, Cu^{2+}, and Fe^{2+}. Since the approach is simple, rapid, and reproducible, a variety of surface-confined CA systems can be prepared.

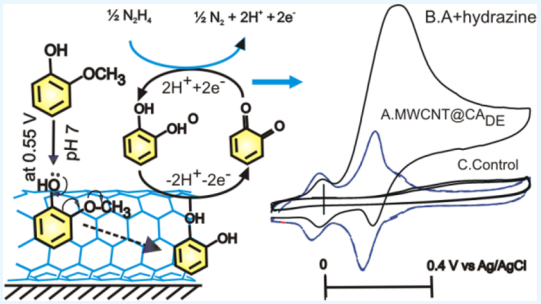

1. INTRODUCTION

Design and development of redox-active organic molecular system functionalized electrodes is a cutting-edge research in bioelectronics,[1,2] bioengineering,[3] biomedical,[4,5] and biosensor[6,7] applications. Since the proton-coupled electron-transfer reaction of catechol is associated with a variety of biomolecular reactions like oxidation of NADH[8,9] and thiol[10,11] and in the neurosignaling system,[12] development of the catechol-based surface-bound thin film as a model bioengineering system is an important research work. Since 1978, there has been immense interest in the development of stable and redox-active surface-confined catechol systems.[13] The following are the representative examples for the preparation of surface-confined CAs: (i) covalent immobilization on the carbon surface; (a) amidation of catechol by chemically reacting it with dicyclohexyl carbodiimide and carboxylic acid functionalized GCE in the triethylamine medium at room temperature,[13,14] wherein the active GCE surface was achieved by treatment with radio-frequency plasma and preanodization procedures, (b) electrochemical functionalization of aldehyde bearing catechol on the preanodized GCE surface under alkaline conditions,[15,16] (c) diazonium-ion-based coupling reactions by chemical (bulk-reaction)[17,18] and electrochemical (surface-reaction) approaches[19−22] and (d) Michael addition reaction based C−C bond formation,[23,24] and (e) a carboxylate linkage by electrochemical reaction of CA with a carboxylic acid functionalized GCE;[25,26] (ii) self-assembled monolayer approach, wherein thiol-functionalized CA derivatives are exposed to a clean gold electrode overnight;[22,27] (iii) oxidative chemisorption of catechol as an ad-layer at a defect-free Pt(111) single-crystal electrode surface in 0.5 M H_2SO_4;[28] (iv) $\pi-\pi$ bonding of sp^2 carbon of catechol with graphitic structure carbon nanomaterials, like MWCNT;[24,29,30] (iv) CA pendant

Received: April 21, 2020
Accepted: June 5, 2020
Published: June 22, 2020

https://dx.doi.org/10.1021/acsomega.0c01846
ACS Omega 2020, 5, 16208−16219

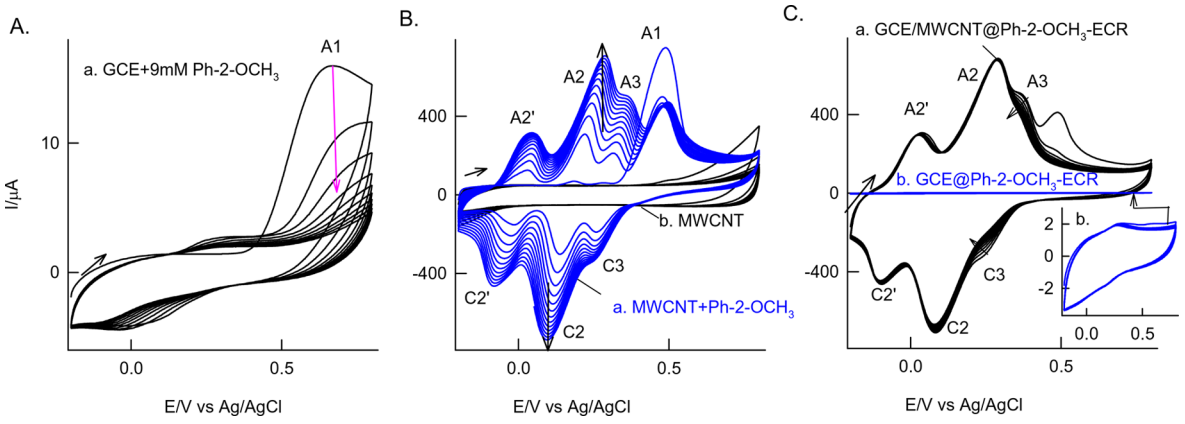

Figure 1. Twenty continuous CV responses of (A) the GCE and (B) GCE/MWCNT with 9 mM Ph-2-OCH_3 and (C) the Ph-2-OCH_3 exposed GCE/MWCNT (MWCNT@Ph-2-OCH_3-ECR) (a) and GCE (GCE@Ph-2-OCH_3-ECR) (b) in pH 7 PBS at ν = 50 mV s^{-1}. (B) curve b is a control CV response of the GCE/MWCNT in pH 7 PBS at ν = 50 mV s^{-1}. ECR = electrochemical reaction product.

metal complex modified electrodes;[31] and (v) catechol-functionalized polymer-modified electrode.[32] It is noteworthy that most of the existing procedures were associated with time-consuming multistep preparation procedures along with the usage of harsh chemicals like concentrated acid or alkaline solution. In all the above cases, achieving a good stability of the surface-confined system is a challenging task. For instance, dicyclohexyl carbodiimide assisted covalent linkage like the catechol-GCE-modified electrode showed about 20% surface fouling in 10 continuous CV experiments in pH 7 phosphate buffer solution (PBS).[14] Similarly, a library of 26 catechol derivatives covalently linked through ethylenediamine and C_6H_4-CH_2-NH linker on the GCE, which has been prepared by a five-step synthetic procedure (~20 h working time), namely; (i) grafting of the *N-tert*-butoxycarbonylamino-ethyl-amine (Boc) spacer on the GCE, (ii) covalent attachment of $C_6H_4CH_2NHBoc$ to the GC surface, (iii) Boc-deprotection of the modified GCE, (iv) coupling reaction of acyl chloride at the GCE, and (v) deprotection of dimethoxy groups at the GCE, showed about 60% fouling of the redox peak within the 10th redox cycling experiment in pH 7 PBS.[21] Herein, we first report a bias-potential-assisted electrochemical reaction of 2-methoxyphenol (guaiacol, as a precursor) to catechol as a stable and highly redox-active surface-confined system on the multiwalled carbon nanotube (MWCNT) surface in neutral pH solution.

Demethylation of organic compounds is one of the critical steps in organic synthesis to prepare several industrially important organic compounds like phenols, guaifenesin, etc.[1,33−35] In general, this functional group transformation is performed under harsh chemical conditions along with strong reagents, for instance, a concentrated H_2SO_4, HI, and H_2O_2 mixture-based demethylation reaction of azodicarboxylates to noroxymophone.[36,37] Similarly, extreme temperatures, 700−800 K, and oxygen-gas-assisted conversion of 2-methoxyphenol to catechol (CA), pyrocatechol (Pyr), methyl catechol, and cresol were also reported.[38] Further, homogeneous catalysts like K_2CO_3 and $Ca(OH)_2$ at high pressure (90 MPa) and high temperature (573 K),[39] a heterogeneous catalyst such as Al_2O_3 and ZSM-5,[40] a supported catalyst with Ni and Co at elevated temperature,[41] and enzyme catalysts based on cytochrome c[42] and horseradish peroxidase (HRP)[43] were reported for the demethylation of guaiacol (Ph-2-OCH_3) to the catechol conversion reaction. In this work, a bias-assisted one-step electrochemical demethylation of guaiacol to surface-confined catechol in mild aqueous solution within 10 ± 0.5 min of preparation time is reported.

In the literature, there are very few reports on the electrochemical demethylation of methoxyphenol in aqueous solutions. In 1973, Adam's group reported a two-step electrochemical procedure involving coulometric oxidation of 2-methoxyphenol at 0.9 V (equivalent of 2 electrons per mole) followed by reduction at 0 V vs Ag/AgCl (equivalent to 0.91 electrons per mole) at carbon paste and porous graphite electrodes for the formation of catechol in the 2 M $HClO_4$ medium.[44] In 2016, Shao et al. reported Ti/Sb-SnO_2 and Ti/Pb_3O_4 anodes for the mineralization of methoxyphenol at about 2 V vs Ag/AgCl in the presence of 5% $NaSO_4$ and NaCl electrolyte solutions.[45] Meanwhile, owing to the antioxidant property of 2-methyoxyphenol,[46,47] there are some electrochemical sensors for the compounds that were developed utilizing the irreversible electrochemical oxidation of phenol. The following are some of the representative electrochemical sensors for the 2-methoxyphenol: graphene sheets-Nafion-Au electroplated screen-printed carbon electrode,[48] sodium gallate exfoliated graphene-nanosheet-modified GCE,[49] MnO_2-graphene oxide modified GCE,[50] γ-Al_2O_3-modified GCE,[51] and biosensors based on HRP,[43] laccase,[52,53] and cytochrome c.[41] In this work, a systematic study has been carried out for the preparation and characterization of MWCNT-surface-confined catechol via voltage-bias-assisted electrochemical demethylation of 2-methoxyphenol in pH 7 PBS. The surface-confined catechol was confirmed by collective physicochemical (FTIR, Raman, UV−vis spectroscopy), molecular (nuclear magnetic resonance and mass spectrometer), and electrochemical characterization techniques. As a model system, stable and highly efficient electrocatalytic oxidation of hydrazine, one of the hazardous substances present in the environment and has been referred as a group B2 carcinogen[54] by the surface-confined catechol system, was demonstrated.

2. RESULTS AND DISCUSSION

2.1. Electrochemical Reaction of 2-Methoxyphenol on Carbon Electrodes. For understanding the basic electrochemistry of 2-methoxyphenol (Ph-2-OCH_3), initial experiments were performed on the bare GCE surface. Figure 1A shows the 10 continuous CV responses of an unmodified GCE in the presence of 9 mM Ph-2-OCH_3 in pH 7 PBS. In the

https://dx.doi.org/10.1021/acsomega.0c01846
ACS Omega 2020, 5, 16208−16219

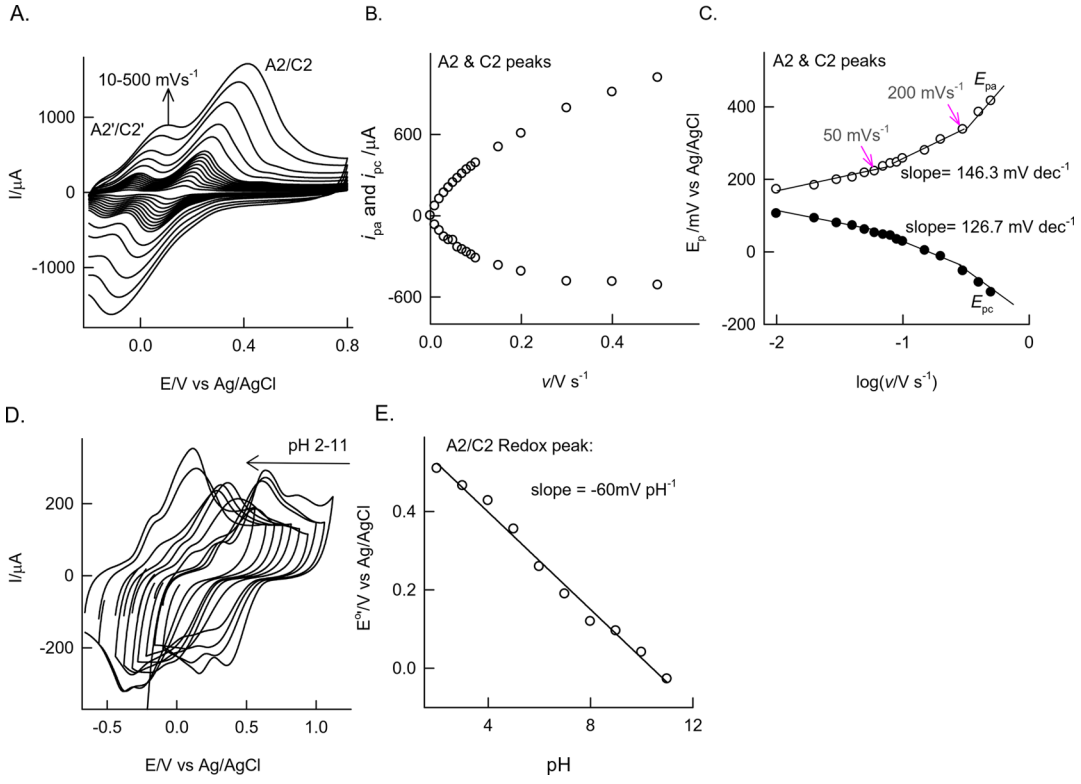

Figure 2. (A) Effect of the scan rate on the CV response of GCE/MWCNT@Ph-2-OCH_3-ECR in pH 7 PBS. Plots of (B) anodic peak current (i_{pa}) and cathodic peak current (i_{pc}) vs scan rate and (C) E_{pa} and E_{pc} vs log of scan rate for peak A2/C2. (D) Effect of pH on the CV response of GCE/MWCNT@Ph-2-OCH_3-ECR at a fixed ν = 50 mV s^{-1}. (E) Plot of $E^{o'}$ vs solution pH.

first cycle, there is an irreversible peak at 0.6 V vs Ag/AgCl (A1 peak) on the anodic side, and the absence of any current peak on the cathodic side was noticed.

Upon increasing the cycle number, a sharp decrement in the current response was observed, and at the 10th cycle, a complete disappearance of the A1 peak was obtained. During the electrochemical cycling process, a feeble redox peak at $E^{o'}$ = 0.15 (A2/C2) V vs Ag/AgCl was observed. After this experiment, when the electrode is gently washed with double distilled water and medium-transferred from Ph-2-OCH_3 to a blank pH 7 PBS and the continuous CV response is measured, there is no sign of the faradaic process. These results indicate the nonamenable characteristics of the Ph-2-OCH_3 on solid electrodes. As a model system, the same CV experiment was performed on the MWCNT-modified GCE, GCE/MWCNT with 9 mM Ph-2-OCH_3 in pH 7 PBS as shown in Figure 1B. Similar to the GCE, an irreversible peak at 0.6 V (A1) in the first cycle was observed. Interestingly, upon successive cycles, specific growth like redox peaks at $E^{o'}$, −0.05 (A2'/C2'), 0.15 (A2/C2), and 0.30 V vs Ag/AgCl (A3/C3), were noticed. At 10th cycles, near saturation in the peak current response was noticed. Unlike the GCE case, when the Ph-2-OCH_3 exposed GCE/MWCNT was medium-transferred to a new pH 7 PBS and 10 continuous CV cycles were performed, the redox peaks, A2/C2 and A2'/C2', were retained without any alteration in the peak current and peak potential. Calculated relative deviation (RSD) and surface-excess values are 1.1% and 16.65 × 10^{-9} mol cm^{-2} (Figure S1), respectively. This observation highlights the uniqueness of the graphitic carbon material on the electrochemical performance of the Ph-2-OCH_3 in a neutral pH solution. This point onward, the electrochemically modified electrode is tentatively designated as GCE/MWCNT@Ph-2-OCH_3-ECR (−OCH_3 = −OMe), wherein ECR means the electrochemical reaction product.

To understand the mechanism of the redox process, GCE/MWCNT@Ph-2-OCH_3-ECR was subjected to the effect of the scan rate experiment in pH 7 PBS (Figure 2A). A regular increase in the redox peak current upon the increase in the scan rate was noticed. A plot of anodic and cathodic peak currents i_{pa} and i_{pc} vs scan rate is linear up to a scan rate of 200 mV s^{-1} indicating the adsorption-controlled electron-transfer feature of the Ph-2-OMe-ECR-modified electrode. The nonlinear characteristic at ν > 200 mV s^{-1} is due to some kinetic restriction. Presumably, owing to a multilayer existence, there is mixed adsorption-diffusion-controlled electron-transfer behavior of the surface-confined redox couple. The electrochemical kinetics parameters were evaluated using the following Laviron model equation:[55,56]

$$SLP_a/SLP_c = \alpha/1 - \alpha \quad (1)$$

$$\log k_s = \alpha \log(1-\alpha) + (1-\alpha)\log \alpha - \log[RT/nF\nu] - \alpha(1-\alpha)nF\Delta E_p/2.303RT \quad (2)$$

where SLP_a and SLP_c are the slopes of E_{pa} (166.3 mV dec^{-1}) and E_{pc} vs log ν plot (126.7 mV dec^{-1}), respectively, α is the transfer coefficient, and ΔE_p is peak-to-peak separation (212 mV) at a scan rate (ν) (100 mV s^{-1}). After substituting the values in eqs 1 and 2, the kinetics parameters, α and k_s values, were calculated to be 0.53 and 1.31 s^{-1}, respectively. The obtained α value, 0.53, is closer to the ideal value, 0.5, indicating a symmetrical energy barrier for the electron-transfer reaction. The k_s value calculated in this work is comparable with previous literature reports of various preparation methods

https://dx.doi.org/10.1021/acsomega.0c01846
ACS Omega 2020, 5, 16208−16219

of surface-confined catechol, namely, self-assembled monolayer (1.1−2.7 s^{-1}),[26] graphite (4 s^{-1}),[26] ferrocene-terminated alkene thiol on Au (SAM) (1.8 s^{-1}),[26] carbon via diazonium coupling (0.87 s^{-1}),[19] and Michael addition reactions (9.8 s^{-1}).[24] Similarly, the surface-excess value obtained, 16.65 × 10^{-9} mol cm^{-2}, is about 10−1000 times higher than the previous literature reports.[10,14,24,57]

Figure 2D shows a typical CV response of the GCE/MWCNT@Ph-2-OCH_3-ECR over a wide range of solution pH (2−11) at a fixed scan rate, 50 mV s^{-1}. A systematic shift in the redox peak potential against changes in the solution pH was noticed. Figure 2E shows a plot of $E^{o'}$ vs pH showing linearity in pH window 2−11 with a slope ($\partial E^{o'}/\partial$pH) value of −60 mV pH^{-1}. This observation denotes the Nernstian type of proton-coupled electron-transfer reaction with participation of an equal number of protons/electrons in the reaction mechanism.

In this stage, it is difficult to predict the actual active species of the Ph-2-OCH_3-ECR. It can be speculated that the demethylation type of functional group transformation happens,[33−40] with the formation of the surface-confined catechol molecule upon the electrochemical experiment. Indeed, since the amount of adsorbed molecule is very less, in the nanogram level, it is a highly challenging task to precisely identify the surface-bound organic species in the chemically modified electrode. To solve the problem and to determine the precise molecular structure of the surface-bound organic species, several critically designed electrochemical and physicochemical characterizations were performed, and the results are summarized below.

2.2. Electrochemical Characterization of GCE/MWCNT@Ph-2-OCH_3-ECR. To identify the key bias potential for the electrochemical preparation of the GCE/MWCNT@Ph-2-OCH_3-ECR, the effect of the potential window (−0.2 to 0.8 V) was investigated at a fixed scan rate, 50 mV s^{-1}, as shown in Figure 3A,B. In the first step (step 1) of experiments, ending potential (E_{final}), −0.8 V, was fixed and the starting potential ($E_{Initial}$) was varied, 0.4 (a), 0.2 (b), 0 (c), and −0.2 V vs Ag/AgCl (d). Similarly, in the step-2 experiments, $E_{Initial}$ was fixed at −0.2 V and E_{final} was varied, 0.4 (a), 0.5 (b), 0.6 (c), and 0.8 V vs Ag/AgCl (d). In the first step-1 experiments, there are no obvious changes in the electrochemical pattern. On the other hand, the step-2 experiments show a clear indication that the anodic sweeping potential 0.5 V vs Ag/AgCl, wherein the A1 irreversible peak operates, is responsible for the formation of the A2/C2 redox peak in this work.

Figure 4 shows the effect of various carbon nanomaterials like carbon black (a bulk carbon material with a mixture of amorphous, crystalline, and graphitic structures), graphitized mesoporous carbon (contains both graphitic units and a ∼50 nm mesoporous structure to entrap organic molecules), single-walled carbon nanotube (allotropes of the MWCNT, contains single units of the CNT), and graphene oxide (possesses rich C−O functional groups) that were modified on the GCE and subjected to electrochemical reaction as mentioned in Figure 1B. Obtained electrochemical patterns are displayed in Figure 4A−D. Figure 4E shows the respective plot of A2-peak current vs carbon nanomaterial. Based on the obtained results, the following summary can be made: (i) all the carbon material showed a qualitatively similar electrochemical reaction to the Ph-2-OCH_3 molecules but to a different extent; (ii) the lowest peak current values are obtained with GO- and SWCNT-modified electrodes suggesting that oxygen-functionalized carbon units hinder the stability of the Ph-2-OCH_3-ECR

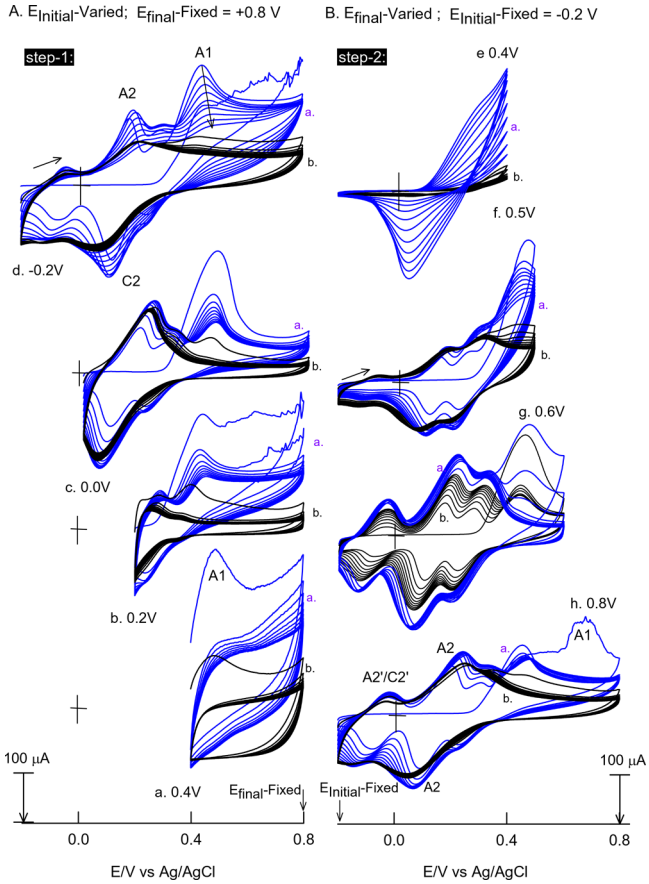

Figure 3. Effect of potential on the continuous CV response of the GCE/MWCNT (freshly prepared electrodes) with 9 mM Ph-2-OCH_3 in pH 7 PBS at ν = 50 mV s^{-1}. (A) CV experiments with a fixed final potential of 0.8 V and varying switching initial potentials of (a) 0.4, (b) 0.2, (c) 0, and (d) −0.2 V vs Ag/AgCl (step 1). (B) CV experiments with a fixed initial potential of −0.2 V and varying final potentials of (e) 0.4, (f) 0.5, (g) 0.6, and (h) 0.8 V vs Ag/AgCl (step 2).

compound formed on the surface and the multilayer graphitic unit rich CNT is suitable for the favorable molecular transformation. Likely, the dense sp^2 graphitic site of the MWCNT is an advantage for strong $\pi-\pi$ interaction with the aromatic structure of the Ph-2-OCH_3 precursor and further to a diffusion-restricted electrochemical reaction. (iii) The porous structure of the carbon units is not encouraging for the stabilization of the surface-confined organic product. With all the speculative information about the product, the Ph-2-OCH_3-ECR is further subjected to physicochemical characterizations as follows.

2.3. Physicochemical Characterization of MWCNT@Ph-2-OCH_3-ECR. Transmission electron microscopy was used to further understand the surface characteristic features of the MWCNT before and after electrochemical treatment with Ph-2-OCH_3 as shown in Figure 5. A black cloud-like morphology with a relatively intense black-colored tubular structure was noticed. Although there is no structural information about the Ph-2-OCH_3-ECR compound, the obtained result may indicate the existence of strong $\pi-\pi$ interaction between the sp^2 site of the MWCNT and aromatic unit of the Ph-2-OCH_3. To substantiate the observation, the modified electrode was subjected to Raman spectroscopic characterization along with a control experiment. For practical convenience, screen-printed

https://dx.doi.org/10.1021/acsomega.0c01846
ACS Omega 2020, 5, 16208−16219

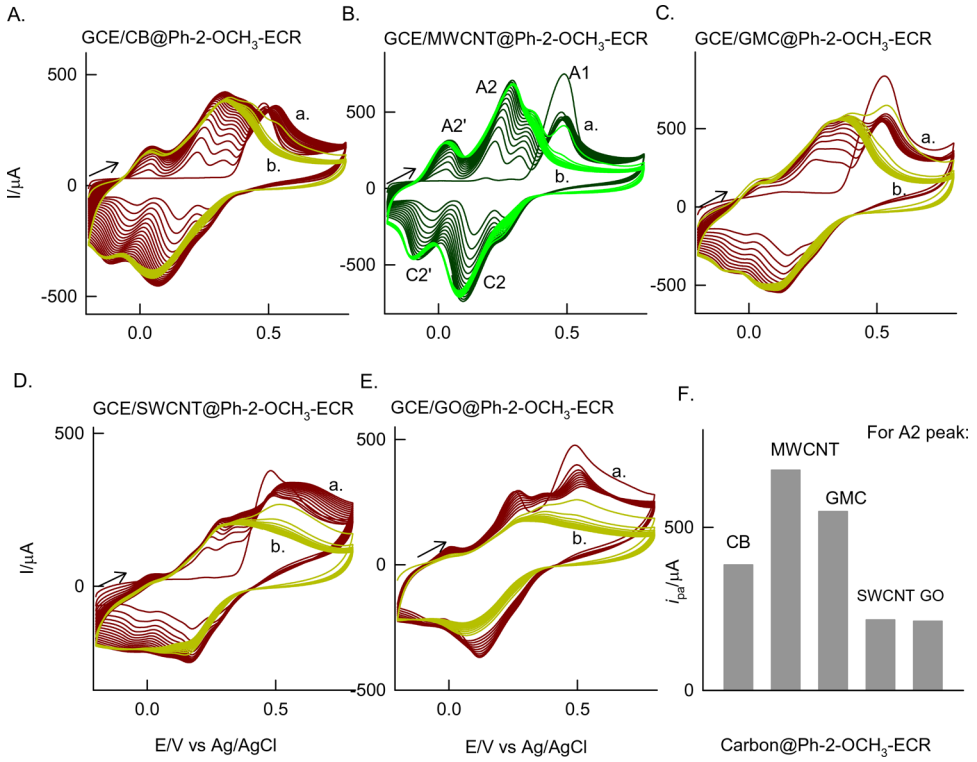

Figure 4. (A–E) CV responses of various carbon-matrix-modified GCEs with (a) 9 mM Ph-2-OCH_3 and (b) their medium-transferred responses in pH 7 buffer solution at ν = 50 mV s^{-1}. (F) Comparison plot of i_{pa}/μA (A2 peak) versus various carbon matrixes. Carbon black = CB, multiwalled carbon nanotube = MWCNT, graphitized mesoporous carbon = GMC, single-walled carbon nanotube = SWCNT, and graphene oxide = GO. ECR = electrochemical reaction product.

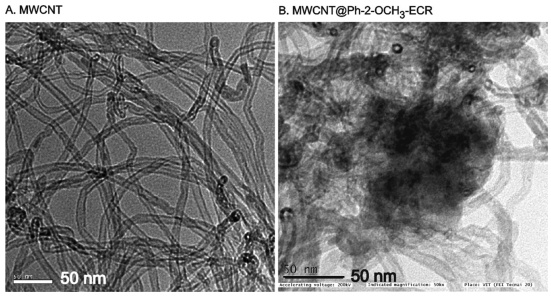

Figure 5. TEM images of (A) the unmodified MWCNT and (B) MWCNT@Ph-2-O-CH_3-ECR.

carbon-modified electrodes were used in this study. As displayed in Figure 6A, both MWCNT and MWCNT@Ph-2-OCH_3-ECR showed a qualitatively similar pattern with the observation of a D-band (disordered graphitic structure due to the sp^3 carbon unit) and G-band (graphitic structure due to the sp^2 carbon site) at 1350 and 1570 cm^{-1}, respectively.

The intensity ratio of the band, I_D/I_G, can be considered as an indication for the alteration in the graphitic surface feature. Calculated I_D/I_G values for the MWCNT and MWCNT@Ph-2-OCH_3-ECR are 0.45 and 0.87, respectively. The marked increment in the ratio is evidence for relatively higher sp^3 content with MWCNT@Ph-2-OCH_3-ECR than that of the MWCNT. This observation supports the association of oxygen-functionalized aromatic molecules like catechol and other polyphenols on the surface-confined system. Further, to strengthen the result, UV–vis and FTIR characterizations were performed as shown in Figure 6B,C. For these experiments, an ethanolic extract of the GCE/MWCNT@Ph-2-OCH_3-ECR was collected by sonicating the modified electrode in 500 μL of ethanol followed by syringe (0.2 μm) filtration and drying and further subjected to chemical characterization without and with a suitable solvent. As can be seen in Figure 6B, a characteristic λ_{max} peak at 286 nm disappeared entirely with the formation of new electronic transitions at 249 (carbonaceous fraction) and 293 nm due to functional group transformation on the electrochemical process. Further characterization studies are needed to confirm the true species. FTIR of the extracted sample showed a specific signal at 1626 cm^{-1} due to the aromatic quinone, whereas the phenolic functional group exhibited a signal at 1589 cm^{-1} (Figure 6C).[58] These characterization results provide preliminary evidence for the conversion of the Ph-2-OCH_3-ECR to polyphenols like organic compounds (CA, HQ-hydroquinone, and pyrogallol) upon the electrochemical reaction. Further, the ethanolic extract was subjected to GC–MS analysis in comparison with a control sample (Ph-2-OCH_3, calculated molecular mass, 124.14) as shown in Figure S2A,B. The control sample showed a characteristic m/z value at 124.14 for the Ph-2-OCH_3 (calculated molecular mass, 121.13), whereas the Ph-2-OCH_3-ECR sample gave m/z peaks at 110.3 (catechol or hydroquinone; calculated molecular mass, 110.1) and 123.16 (pyrogallol, calculated molecular weight, 126.11; [M–3H] peak; it may be formed as a fragmentation pathway molecule). To authenticate the expectation, the ethanolic extracted sample (Ph-2-OCH_3-ECR) was further subjected to NMR measurement. Depending upon the nature of protons and different chemical environments present, the proton will resonate either downfield or upfield within the NMR spectrum. Proton NMR can be used to easily differentiate catechol over HQ. In catechol, due to *ortho-*

https://dx.doi.org/10.1021/acsomega.0c01846
ACS Omega 2020, 5, 16208–16219

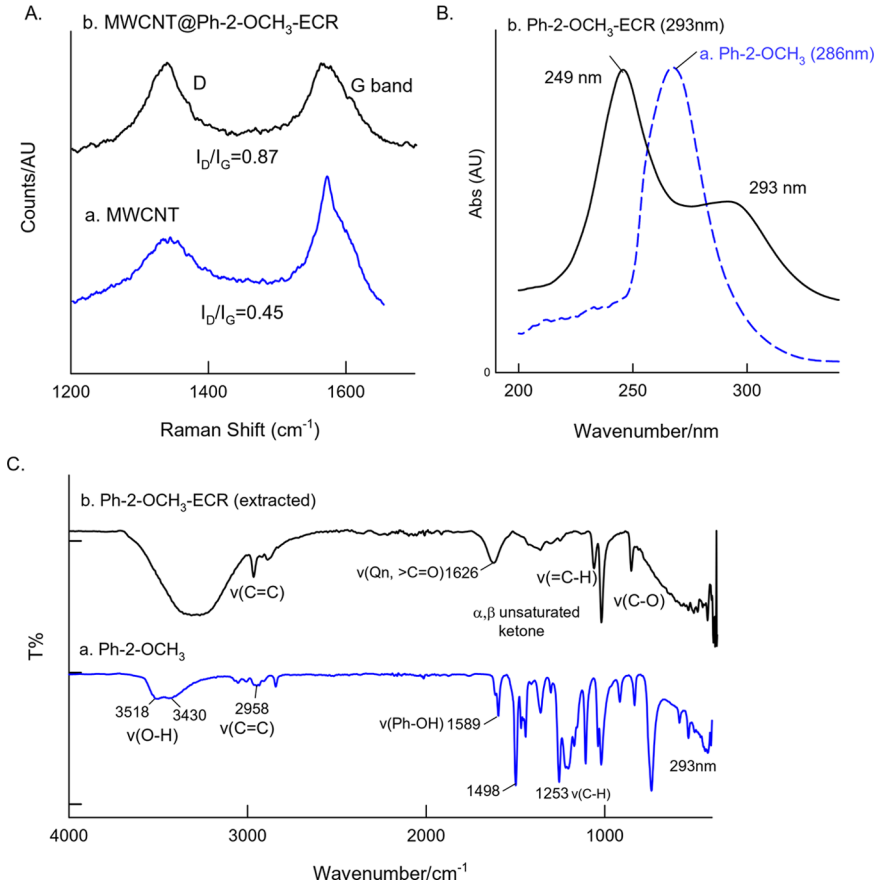

Figure 6. Comparative characterization of the MWCNT@Ph-2-OCH$_3$-ECR with control samples by (A) Raman, (B) UV−vis, and (C) FTIR spectroscopic analysis. For Raman analysis, samples were prepared on a disposable screen-printed electrode as an underlying surface. The MWCNT@Ph-2-OCH$_3$-ECR sample was extracted from the test electrode using ethanol as a solvent.

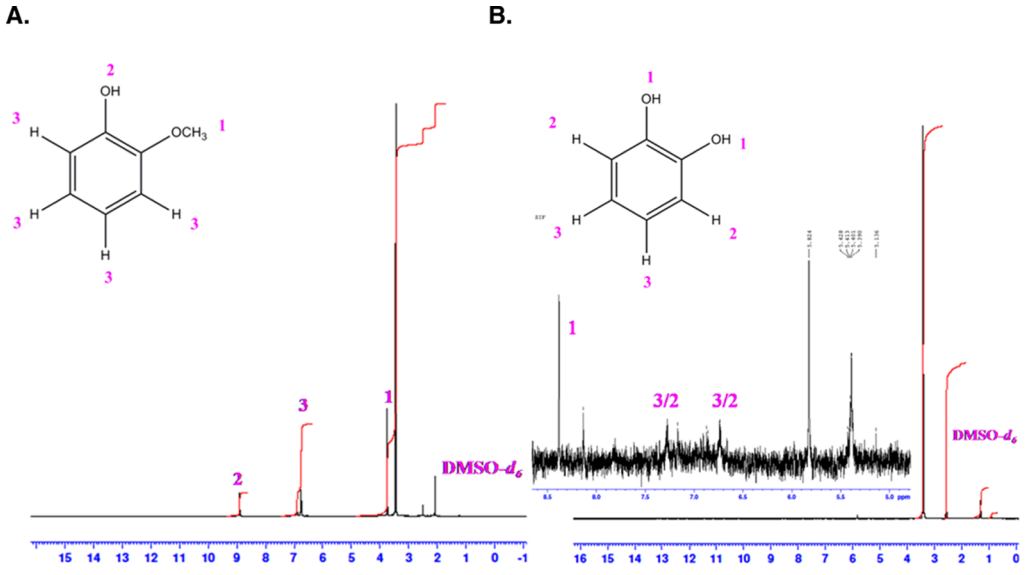

Figure 7. NMR spectra of (A, control) the Ph-2-OCH$_3$ and (B) Ph-2-OCH$_3$-ECR obtained from the cycling voltammetry (GCE/MWCNT with Ph-2-OCH$_3$). Insets are typical illustrations of respective organic compounds and their positions.

and *meta*-coupling, aromatic protons appear as a multiplet, and it will resonate at the downfield in the aromatic region. On the other hand, in HQ, due to molecular symmetry, aromatic protons appear as a singlet in the NMR spectrum. Prior to the analysis, the small amount of sample was purified using a column filter in a pipette column, and later, the thin-layer chromatographic method was run as displayed in Figure S3. Meanwhile, for qualitative comparison, catechol and pyrogallol samples (controls) were placed in the TLC plate, and their retention factors (R_f) were analyzed. It is interesting to notice that the R_f values match between the Ph-2-OCH$_3$-ECR and catechol. Figure 7A,B shows the typical DMSO-d_6 NMR

https://dx.doi.org/10.1021/acsomega.0c01846
ACS Omega 2020, 5, 16208−16219

Scheme 1. Illustration of Graphitic-Surface-Assisted Electrochemical Demethylation of Ph-2-OCH_3[a]

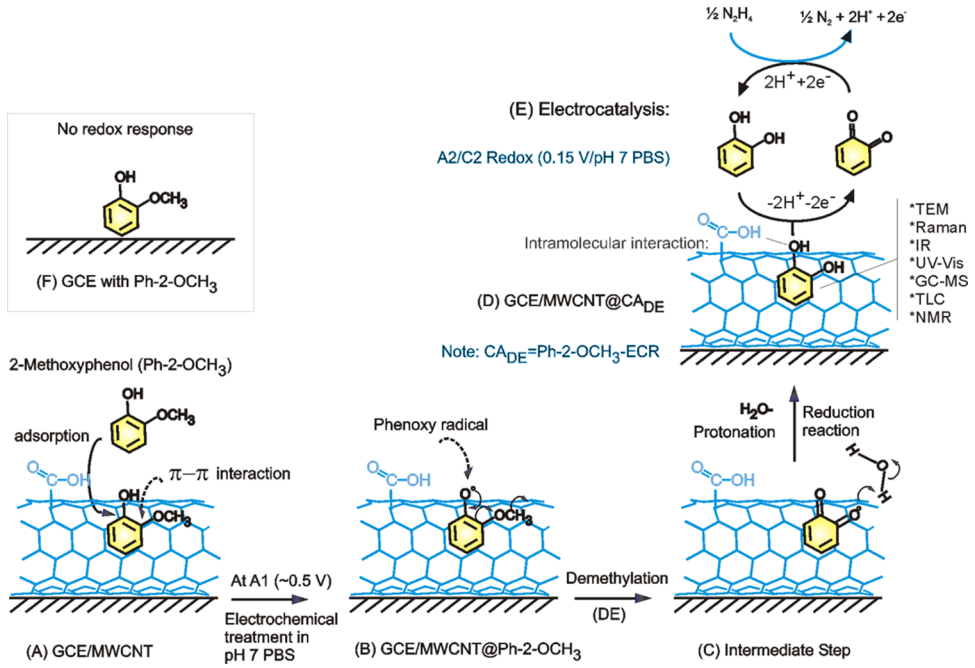

[a](A) Electrochemical oxidation step at the A1-peak potential, (B) typical demethylation step on the graphitic surface, and (C) protonation and reduction of the intermediate (other details in Scheme 2). (D) MWCNT-surface-confined catechol molecule and its redox and electrocatalytic mechanism. The inset shows an illustration of the interaction of the GCE with Ph-2-OCH_3. ECR = electrochemical reaction product. CA_{DE} = 2-methoxyphenol demethylated (DE) product, catechol (CA). (F) Illustration of the nonreactive interaction between Ph-2-OCH_3 and bare GCE surface.

spectra of Ph-2-OCH_3 (control) and the TLC-extracted Ph-2-OCH_3-ECR samples. NMR signals (δ) in ppm noticed with the control, Ph-2-OCH_3, are 8.9 (C2; s, 1H of OH), 6.8 (C3; multiplet, 4H, phenyl), and 3.7 (C1; singlet, 3H, $-OCH_3$), whereas in the case of Ph-2-OMe-ECR, DMSO-d_6 NMR signals (in ppm) are 8.4 (C1; singlet; OH) and 6.8−7 (C2 and C3; multiplet; 4H, phenyl). In view of the presence of the characteristic proton signals, we can conclude that catechol (Ph-2-OMe-ECR) was a chief product and can conclusively rule out the HQ and pyrogallol existence.

To confirm this observation, commercial CA and pyrogallol (control) samples prepared as a solution in ethanol were adsorbed on the MWCNT, and the CV responses were measured (Figure S4). It is obvious that the A2/A2 and A2'/C2' noticed in this work merely match with those of the control sample of CA, not with the pyrogallol's. The minor A2'/C2' redox signal seen in this work is attributed to surface confinement of the CA at energetically different carbon sites.[28] This point onward, the GCE/MWCNT@Ph-2-OCH_3-ECR is redesignated as GCE/MWCNT@CA_{DE}, wherein CA_{DE} is electrochemically demethylated Ph-2-OCH_3 to CA product. Based on the electrochemical and physicochemical characterization results, it is proposed that upon electrochemical potential cycling of the GCE/MWCNT, the solution phase Ph-2-CH_3 was adsorbed on the numerous graphitic sites of the MWCNT through $\pi-\pi$ interaction and involved in electrochemical oxidation of the phenolic site as a first step followed by radical delocalization, protonation, and then a water addition step for the formation of a surface-confined CA. The details of the overall mechanism and step-by-step molecular transformation information are sketched in Schemes 1 and 2, respectively.

Scheme 2. Plausible Electrochemical Oxidation Mechanism for the Demethylation of Redox-Inactive Ph-2-OCH_3 (Guaiacol) to Redox-Active Catechol (Ph-2-OCH_3-ECR) on the GCE/MWCNT-Modified Electrode System via Generation of a Phenoxy Radical, Protonation, Reduction Reactions in pH 7 Phosphate Buffer Solution. Ph-2-OCH_3-ECR = Catechol

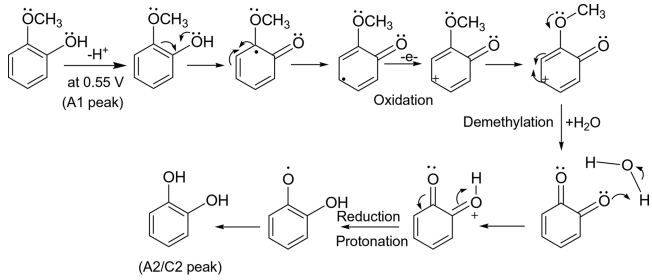

2.4. Electrocatalytic Hydrazine Oxidation and Sensing. The hydrazine oxidation reaction was studied as a model system for the mediation of the proton-coupled electron-transfer reaction of catechol in a neutral pH solution. Figure 8A, curves a and b, shows 2 mM hydrazine electrochemical oxidation reactions at the GCE/MWCNT and GCE/MWCNT@CA_{DE}. The unmodified electrode failed to show any electrochemical oxidation signal in the tested potential window, whereas the MWCNT@CA_{DE}-modified electrode showed a profound anodic signal at the anodic peak potential, 0.22 V, near to the existence of the A2/C2 redox couple. The oxidation current signal obtained at the CA_{DE}-modified electrode is about 400 times higher than and shows 500 mV reduction in the potential compared to the respective values

https://dx.doi.org/10.1021/acsomega.0c01846
ACS Omega 2020, 5, 16208−16219

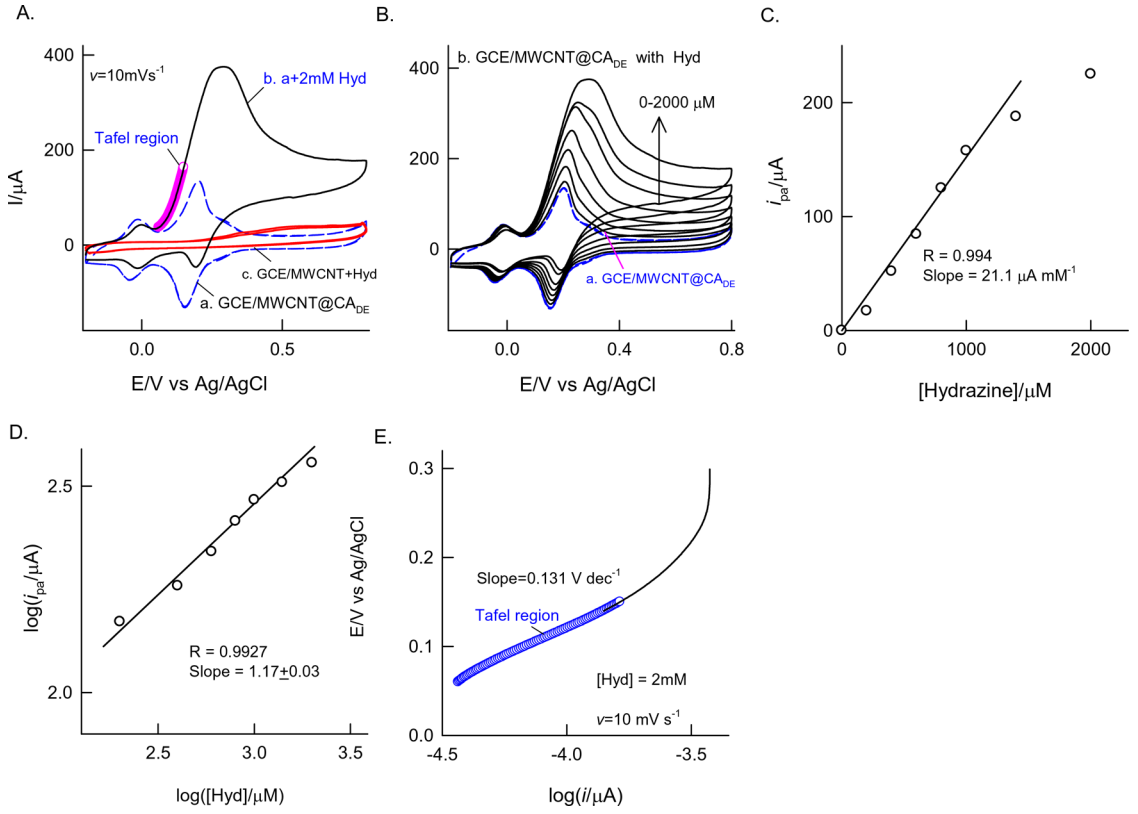

Figure 8. (A) CV responses of GCE/MWCNT@CA_{DE} (a) without and (b) with 2 mM hydrazine at v = 10 mV s^{-1} in pH 7 PBS. The inset plot is a Tafel region. Curve c is a control CV of the GCE/MWCNT with 2 mM hydrazine. (B) Effect of hydrazine concentration on the CV response of GCE/MWCNT@CA_{DE} at v = 10 mV s^{-1} in pH 7 PBS. Plots of (C) i_{pa} vs Hyd concentration, (D) log i_{pa} vs log[Hyd], and (E) E vs log i (Tafel plot).

Table 1. Comparative Electroanalytical Performance for Hydrazine Detection Using GCE/MWCNT@Ph-2-OCH_3-ECR with Some Representative Literature Reports (Based on the CV Result)[a]

	chemically modified electrode	pH	E_{pa}/V vs Ag/AgCl	sensitivity (μA mM^{-1})	linear range (mM)	ref
1	GCE/CNT@CA-deriv.	4−8, PBS	0.25	0.76−3.05	0.002−4.5	29
2	GCE/MWCNT@EA	7, PBS	0.2	22.8	0.5−9	56
3	GCE/PB	3, 0.1 M K_2SO_4	0.9	22.6	0−100	59
4	GCE/CGA	7.5, PBS	0.30	11.0	0−1	60
5	GCE/CNT@PCV	7.5, PBS	0.5	19.8	0.05−4	61
7	GCE/MWCNT@QLO	7, PBS	0.10	4.4	0−10	62
8	GCE/MWCNT@PQQ	7, Tris buffer	0.45	1.0	0−10	63
9	GCE/CNT@HQ (HQ-hydroquinone)	7, PBS	0.3	2.06	0−10	64
10	GCE/MWCNT@CA_{DE}	7, PBS	0.15	21.1	0−1	our work

[a]PB = Prussian blue; CA-deriv. = catechol derivatives, catechin hydrochloride, chlorogenic acid, and caffeic acid; PCV = pyrocatechol violet; EA = ellagic acid; HQ = hydroquinone; PQQ = pyrroloquinoline quinone; QLO = quinolone quinones; CA_{DE} = CA derived from demethylation of 2-methoxyphenol on the MWCNT.

obtained with the MWCNT (Figure 8A, curve c). This observation is attributed to the efficient electrocatalytic functionality of the surface-confined CA redox system. Unlike in the literature reports, there is no fouling of the CA upon the electrocatalytic oxidation reaction, highlighting the superior functionality of the present work to the existing literature report. The electrocatalytic hydrazine oxidation was further extended to electroanalytical sensing by CV and amperometric i−t techniques. Figure 8B shows a typical CV response of GCE/MWCMT@CA_{DE} with increasing concentration of hydrazine in the window of 0−1 mM at a fixed scan rate, 10 mV s^{-1}. The oxidation current signal was linear with hydrazine concentration in a window of 0−2 mM with a current sensitivity and regression coefficient values of 21.1 μA mM^{-1} and 0.9991, respectively (Figure 8C). A comparative table for different hydrazine sensors reported is tabulated in Table 1 showing appreciably good sensitivity at a low detection potential.[29,56,59−64] A double logarithmic plot of i_{pa} vs [Hyd] is linear, with a slope value of 1.16 attributed to the first-order reaction rate for the oxidation reaction. A Tafel plot was constructed using the increasing portion of the hydrazine (2 mM) oxidation current curve as shown in Figure 8D,E. The calculated anodic Tafel slope (b_a) for the hydrazine oxidation reaction is 131 mV dec^{-1}. Assuming that the number of electrons transferred (n_a) involved in the rate-determining step

https://dx.doi.org/10.1021/acsomega.0c01846
ACS Omega 2020, 5, 16208−16219

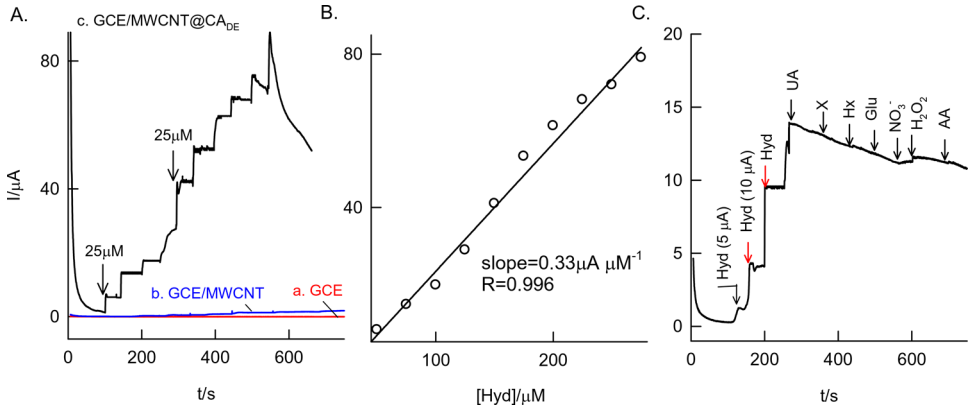

Figure 9. (A) Comparative amperometric $i-t$ responses of (a) GCE/MWCNT@CA$_{DE}$, (b) GCE/MWCNT, and (c) GCE for continuous sensing of 25 μM hydrazine (final concentration) at an applied potential, 0.15 V vs AgCl in 10 mL of pH 7 PBS (hydrodynamic conditions). (B) Typical calibration plot. (C) Amperometric $i-t$ response of the GCE/MWCNT@CA$_{DE}$ with various interfering chemicals along with hydrazine (Hyd) in pH 7 PBS. UA = uric acid, X = xanthine, Hx = hypoxanthine, Glu = glucose, and AA = ascorbic acid.

is 1 and the relationship $b_a = 2.303RT/(1 - \alpha')n_aF$, the α' value is estimated to be 0.54.

Figure 9A,B shows the amperometric $i-t$ response of continuous spikes of 25μM hydrazine in 10 mL of pH 7 PBS at an applied potential, E_{app} = 0.15 V vs Ag/AgCl. A systematic increase in the sensing current against the hydrazine spikes was noticed. Constructed calibration was linear in a window of 0−300 μM hydrazine with current sensitivity and regression values of 0.33 μA μM^{-1} and 0.9993, respectively (Figure 9C). The calculated detection limit value is 8.8 μM. Interestingly, the electrode was found to be tolerant to interferences of other biochemicals such as uric acid (UA), xanthine (X), hypoxanthine (Hx), glucose (Glu), nitrate (NO^{3-}), hydrogen peroxide (H_2O_2), ascorbic acid (AA), Cu^{2+} (data not enclosed), and Fe^{2+} (data not enclosed). Indeed, the tolerance to interferences was also noticed with dopamine, hydroquinone, and resorcinol that were used as analytes (data not enclosed). Five repeated modified electrode preparations showed an RSD value of 7.5% demonstrating good reproducibility of this new preparation technique.

3. CONCLUSIONS

A new electrochemical approach has been introduced for the preparation of surface-confined catechol on the graphitic carbon electrode using 2-methoxyphenol as a precursor compound in a neutral pH solution. The redox signal is surface-confined in nature, and the activity is Nernstian type of proton-coupled electron transfer. Potential cycling of the MWCNT-modified GCE in a window of −0.2 to 0.8 V in a dilute solution of 2-methoxyphenol resulted in the formation of a stable and well-defined redox couple at $E^{o'}$ = 0.15 (A2/C2) V vs Ag/AgCl with a surface-excess value of 16.65 × 10^{-9} mol cm^{-2}. In order to elucidate the true species, the modified electrode was characterized by several electrochemical and physicochemical techniques based on potential segment CV experiment, TEM, Raman, IR, UV−vis, and NMR spectroscopic analysis. Collecting results from these techniques, it has been revealed that electrochemical-reaction-assisted demethylation of 2-methoxyphenol to catechol occurred on the GCE/MWCNT surface and hence showed the well-defined surface-confined redox signal in this work. As a model system, electrocatalytic oxidation of hydrazine was performed on the new surface-confined catechol system in a neutral pH solution. The electrokinetics parameters such as Tafel slope and transfer coefficient were measured to be 131 mV dec^{-1} and 0.54, respectively. A summary of the new findings in this work is as follows: (i) A new approach for preparation of a stable surface-confined catechol system in neutral pH, unlike the literature report on strong acid or nonaqueous-based preparation conditions. (ii) The new modified electrode is prepared within 10 min, contradictory to the literature reports with a series of synthetic organic steps (covalent modification and diazotization steps) and time-consuming preparation procedures. (iii) This new procedure allows about 10 times higher surface-excess value of surface-confined catechol than that of the conventional preparation procedure. (iv) There is no fouling of the catechol unit upon the continuous CV cycling experiment in neutral pH solution unlike the severe fouling noticed with the covalently immobilized catechol-modified electrode, and (v) the efficient electrocatalytic function was demonstrated using hydrazine oxidation as a model system. Hence, the present approach is a superior platform to the existing literature report.

4. EXPERIMENTAL SECTION

4.1. Materials. Guaiacol (>98%, CAS 90-05-1, TCI), graphitized mesoporous carbon (GMC, 99.95%; 50 nm), single-layer graphene oxide ethanol nanodispersed (GO, >80%, 0.6−1.2 nm thickness, 0.5−2.0 μm flake size), single-walled carbon nanotube (SWCNT; ∼70% purity on a carbon basis, size 0.7−1.1 nm diameter), MWCNT (∼95% purity assay; outer diameter size 10−15 nm; inner diameter size 2−6 nm; length 0.1−10 mm), and carbon black (CB, N330 grade gifted by Phillips Carbon Black Ltd., Kochi, India) were used without modification. A 0.1 M ionic strength pH 7 phosphate buffer solution prepared using Na_2HPO_4 and NaH_2PO_4 in double-distilled H_2O was used as a supporting electrolyte. Hydrazine sulfate extrapure AR stored in a brown bottle (SRL, India) was used without any further purification. ***Caution!*** Since hydrazine is suspected as a carcinogenic substance, care must be taken while handling the chemical.

4.2. Apparatus. A CHI electrochemical workstation model 660 C (USA) was used to carry out cyclic voltammetric and differential pulse measurements using a 10 mL working volume cell. A three-electrode system consisting of a glassy carbon electrode (GCE; 3 mm diameter) and its chemically modified

https://dx.doi.org/10.1021/acsomega.0c01846
ACS Omega 2020, 5, 16208−16219

system as a working electrode, Ag/AgCl (in 3 M KCl) as a reference electrode, and platinum disc (2 mm diameter) as a counter electrode was used. Transmission electron microscope (TEM) characterization was done using an FEI-Tecnai G2 20 Twin Instrument using a 3 mm diameter copper grid system. FTIR spectroscopic measurements were performed using a Shimadzu instrument (Japan), and UV−vis spectroscopic studies were done using a JASCO (V-670 PC) 4100 instrument (Japan) with the KBr method. A Horiba XploRA instrument (France) was used for the Raman spectroscopic analysis of the modified electrodes at a fixed wavelength of 532 nm. Gas chromatography−mass spectroscopy for column-filtered extracted ethanolic solution was performed using an Agilent 7890B gas chromatograph instrument. The proton NMR spectrum was recorded on a Bruker 400 MHz using DMSO-d_6 as a solvent. For the NMR analysis, an extracted solution was obtained by sonicating the modified electrode in 500 μL of ethanol and filtering using a syringe filter (0.2 μm) and used.

4.3. Preparation of the Surface-Confined Catechol-Modified Electrode. Initially, the bare GCE was wet-polished using an alumina powder-distilled water suspension using a BAS polishing kit and rinsed off to eliminate residual abrasive particles followed by sonication in double-distilled water for about 2 min. Later, the electrode was electrochemically pretreated (−0.2 to 1.2 V vs Ag/AgCl at a scan rate (ν) of 50 mV s^{-1} for 20 cycles) in pH 7 PBS. Next, 5 μL of 3 mg carbon nanomaterial (carbon nanomaterials like CB, MWCNT, GMC, SWCNT, and GO) dispersed in ethanol (1 mL) was drop-cast on the bare GCE surface and left to dry (25 ± 2 °C) for 2 ± 1 min. Then, the modified electrode was placed in a cell containing 9 mM 2-methoxyphenol in pH 7 PBS, and 20 continuous potential cycling experiments in a window of −0.2 to 0.8 V vs Ag/AgCl at a scan rate ν of 50 mV s^{-1} were performed. It took only 6.6 min to complete the experiment. Such an electrochemical treatment procedure led to the formation of surface-confined catechol on the carbon-nanomaterial-modified GCE surface. As a pretreatment procedure, the as-prepared modified electrode was gently washed with double-distilled water and then medium-transferred to a new pH 7 PBS, and 10 cycles of continuous CV in a potential window of −0.2 to 0.8 V vs Ag/AgCl at ν = 50 mV s^{-1} were performed.

The surface excess Γ of the electroactive redox species responsible was calculated with the equation $\Gamma = QnFA_e$, where Q is the charge, obtained by integrating the anodic redox peak area in the cyclic voltammetry at a slow scan rate, 10 mV s^{-1}, in pH 7 PBS, n is the number of electrons transferred (1 in the present case), and A_e is the electrode geometric area (0.0707 cm^2).

■ ASSOCIATED CONTENT

Supporting Information

The Supporting Information is available free of charge at https://pubs.acs.org/doi/10.1021/acsomega.0c01846.

Figure S1, plot of surface excess vs Ph-2-OCH_3 concentration used in the electrochemical demethylation reaction; Figure S2, GC−MS responses of Ph-2-OCH_3 and Ph-2-OCH_3-ECR; Figure S3, typical thin-layer chromatography of ethanolic extract from MWCNT@Ph-2-OCH_3-ECR with various controls; Figure S4, control CV responses of catechol, pyrogallol, and a mixture of catechol + pyrogallol on the GCE/MWCNT in pH 7 PBS (PDF)

■ AUTHOR INFORMATION

Corresponding Authors

Desikan Rajagopal − *Department of Chemistry, School of Advanced Sciences, Vellore Institute of Technology University, Vellore 632014, India*; Phone: +1-407 590 3978; Email: Desikan.Rajagopal@ucf.edu

Annamalai Senthil Kumar − *Nano and Bioelectrochemistry Research Laboratory, Department of Chemistry, School of Advanced Sciences, Department of Chemistry, School of Advanced Sciences, and Carbon Dioxide Research and Green Technology Centre, Vellore Institute of Technology University, Vellore 632014, India*; orcid.org/0000-0001-8800-4038; Phone: +91-416-2202754; Email: askumarchem@yahoo.com, askumar@vit.ac.in

Author

Mansi Gandhi − *Nano and Bioelectrochemistry Research Laboratory, Department of Chemistry, School of Advanced Sciences and Department of Chemistry, School of Advanced Sciences, Vellore Institute of Technology University, Vellore 632014, India*

Complete contact information is available at: https://pubs.acs.org/10.1021/acsomega.0c01846

Notes

The authors declare no competing financial interest.

■ ACKNOWLEDGMENTS

The authors acknowledge the Department of Science and Technology − Science and Engineering Research Board (DST-SERB-EMR/2016/002818) Scheme. M.G. thanks the Indian Council of Medical Research for the award of her senior research fellowship (2019-4952).

■ REFERENCES

(1) Wu, S.; Kim, E.; Li, J.; Bentley, W. E.; Shi, X.-W.; Payne, G. F. Catechol-Based Capacitor for Redox-Linked Bioelectronics. *ACS Appl. Electron. Mater.* **2019**, *1*, 1337−1347.

(2) Zhang, Y.; Thomas, Y.; Kim, E.; Payne, G. F. PH- and Voltage-Responsive Chitosan Hydrogel through Covalent Cross-Linking with Catechol. *J. Phys. Chem. B.* **2012**, *116*, 1579−1585.

(3) Lee, S.-w.; Ryu, J. H.; Do, M. J.; Namkoong, E.; Lee, H.; Park, K. NiCHE Platform: Nature-Inspired Catechol-Conjugated Hyaluronic Acid Environment Platform for Salivary Gland Tissue Engineering. *ACS Appl. Mater. Interfaces* **2020**, *12*, 4285−4294.

(4) Forooshani, P. K.; Meng, H.; Lee, B. P. Catechol Redox Reaction: Reactive Oxygen Species Generation, Regulation, and Biomedical Applications. In *Advances in Bioinspired and Biomedical Materials*; American Chemical Society: Washington, DC, 2017, *1252*(10), 179−196.

(5) Zhang, Z.; He, X.; Zhou, C.; Reaume, M.; Wu, M.; Liu, B.; Lee, B. P. Iron Magnetic Nanoparticle-Induced ROS Generation from Catechol-Containing Microgel for Environmental and Biomedical Applications. *ACS Appl. Mater. Interfaces* **2020**, 21210.

(6) Winkler, T. E.; Ben-Yoav, H.; Chocron, S. E.; Kim, E.; Kelly, D. L.; Payne, G. F.; Ghodssi, R. Electrochemical Study of the Catechol-Modified Chitosan System for Clozapine Treatment Monitoring. *Langmuir* **2014**, *30*, 14686−14693.

(7) Lebègue, E.; Louro, R. O.; Barrière, F. Electrochemical Detection of pH-Responsive Grafted Catechol and Immobilized Cytochrome c onto Lipid Deposit-Modified Glassy Carbon Surface. *ACS Omega* **2018**, *3*, 9035−9042.

(8) Bonora, M.; Patergnani, S.; Rimessi, A.; De Marchi, E.; Suski, J. M.; Bononi, A.; Giorgi, C.; Marchi, S.; Missiroli, S.; Poletti, F.; et al. ATP Synthesis and Storage. *Purinergic Signal.* **2012**, *8*, 343−357.
(9) Smeitink, J. A.; Zeviani, M.; Turnbull, D. M.; Jacobs, H. T. Mitochondrial Medicine: A Metabolic Perspective on the Pathology of Oxidative Phosphorylation Disorders. *Cell Metab.* **2006**, *3*, 9−13.
(10) Sanada, H.; Nakashima, Y.; Suzue, R.; Kawadai, S. Effect of catechol-Thiol Conjugates on Tyrosinase-Dependent Tyrosine Hydroxylation. *J. Nutr. Sci. Vitaminol.* **1976**, *22*, 389−396.
(11) Boots, A. W.; Haenen, G. R. M. M.; Den Hartog, G. J. M.; Bast, A. Oxidative Damage Shifts from Lipid Peroxidation to Thiol Arylation by Catechol-Containing Antioxidants. *Biochim. Biophys. Acta, Mol. Cell Biol. Lipids* **2002**, *1583*, 279−284.
(12) Parkkila, P.; Viitala, T. Partitioning of Catechol Derivatives in Lipid Membranes: Implications for Substrate Specificity to Catechol-*O*-methyltransferase. *ACS Chem. Neurosci.* **2020**, *11*, 969−978.
(13) Tse, D. C.-S.; Kuwana, T. Electrocatalysis of Dihydronicotinamide Adenosine Diphosphate with Quinones and Modified Quinone Electrodes. *Anal. Chem.* **1978**, *50*, 1315−1318.
(14) Ueda, C.; Tse, D. C.-S.; Kuwana, T. Stability of catechol modified carbon electrodes for electrocatalysis of dihydronicotinamide adenine dinucleotide and ascorbic acid. *Anal. Chem.* **1982**, *54*, 850−856.
(15) Pariente, F.; Tobalina, F.; Darder, M.; Lorenzo, E.; Abruña, H. D. Electrodeposition of Redox-Active Films of Dihydroxybenzaldehydes and Related Analogs and Their Electrocatalytic Activity toward NADH Oxidation. *Anal. Chem.* **1996**, *68*, 3135−3142.
(16) Pariente, F.; Tobalina, F.; Moreno, G.; Hernández, L.; Lorenzo, E.; Abruña, H. D. Mechanistic Studies of the Electrocatalytic Oxidation of NADH and Ascorbate at Glassy Carbon Electrodes Modified with Electrodeposited Films Derived from 3,4-Dihydroxybenzaldehyde. *Anal. Chem.* **1997**, *69*, 4065−4075.
(17) Algharaibeh, Z.; Pickup, P. G. An Asymmetric Supercapacitor with Anthraquinone and Dihydroxybenzene Modified Carbon Fabric Electrodes. *Electrochem. Commun.* **2011**, *13*, 147−149.
(18) Pognon, G.; Cougnon, C.; Mayilukila, D.; Bélanger, D. Catechol-Modified Activated Carbon Prepared by the Diazonium Chemistry for Application as Active Electrode Material in Electrochemical Capacitor. *ACS Appl. Mater. Interfaces* **2012**, *4*, 3788−3796.
(19) Nguyen, N. H.; Esnault, C.; Gohier, F.; Bélanger, D.; Cougnon, C. Electrochemistry and Reactivity of Surface-Confined Catechol Groups Derived from Diazonium Reduction. Bias-Assisted Michael Addition at the Solid/liquid Interface. *Langmuir* **2009**, *25*, 3504−3508.
(20) Hayat, A.; Barthelmebs, L.; Sassolas, A.; Marty, J.-L. An Electrochemical Immunosensor Based on Covalent Immobilization of Okadaic Acid onto Screen Printed Carbon Electrode via Diazotization-Coupling Reaction. *Talanta* **2011**, *85*, 513−518.
(21) Ghanem, M. A.; Chrétien, J.-M.; Kilburn, J. D.; Bartlett, P. N. Electrochemical and Solid-Phase Synthetic Modification of Glassy Carbon Electrodes with Dihydroxybenzene Compounds and the Electrocatalytic Oxidation of NADH. *Bioelectrochemistry* **2009**, *76*, 115−125.
(22) Behera, S.; Sampath, S.; Raj, C. R. Electrochemical Functionalization of a Gold Electrode with Redox-Active Self-Assembled Monolayer for Electroanalytical Application. *J. Phys. Chem. C* **2008**, *112*, 3734−3740.
(23) Rębiś, T.; Sobczak, A.; Wierzchowski, M.; Frankiewicz, A.; Teżyk, A.; Milczarek, G. An Approach for Electrochemical Functionalization of Carbon nanotubes/1-Amino-9,10-Anthraquinone Electrode with Catechol Derivatives for the Development of NADH Sensors. *Electrochim. Acta* **2018**, *260*, 703−715.
(24) Kumar, A. S.; Sornambikai, S.; Gayathri, P.; Zen, J.-M. Selective Covalent Immobilization of Catechol on Activated Carbon Electrodes. *J. Electroanal. Chem.* **2010**, *641*, 131−135.
(25) Ramesh, P.; Sampath, S. Electrochemical and Spectroscopic Characterization of Quinone Functionalized Exfoliated Graphite. *Analyst* **2001**, *126*, 1872−1877.
(26) Nakano, K.; Ohkubo, K.; Taira, H.; Takagi, M.; Imato, T. Electrocatalytic Oxidation of Dihydronicotineamide Adenine Dinucleotide on Gold Electrode Modified with Catechol-Terminated Alkanethiol Self-Assembly. *Anal. Chim. Acta* **2008**, *619*, 30−36.
(27) Rodriguez-Lopez, M.; Rodes, A.; Berná, A.; Climent, V.; Herrero, E.; Tuñon, P.; Feliu, J. M.; Aldaz, A.; Carrasquillo, A. Model System for the Study of 2D Phase Transitions and Supramolecular Interactions at Electrified Interfaces: Hydrogen-Assisted Reductive Desorption of Catechol-Derived Adlayers from Pt(111) Single-Crystal Electrodes. *Langmuir* **2008**, *24*, 3551−3561.
(28) Kumar, A. S.; Swetha, P. Electrochemical-Assisted Encapsulation of Catechol on a Multiwalled Carbon Nanotube Modified Electrode. *Langmuir* **2010**, *26*, 6874−6877.
(29) Salimi, A.; Miranzadeh, L.; Hallaj, R. Amperometric and Voltammetric Detection of Hydrazine Using Glassy Carbon Electrodes Modified with Carbon Nanotubes and Catechol Derivatives. *Talanta* **2008**, *75*, 147−156.
(30) Storrier, G. D.; Takada, K.; Abruña, H. D. Catechol-Pendant Terpyridine Complexes: Electrodeposition Studies and Electrocatalysis of NADH Oxidation. *Inorg. Chem.* **1999**, *38*, 559−565.
(31) Jaegfeldt, H.; Torstensson, A. B. C.; Gorton, L. G. O.; Johansson, G. Catalytic Oxidation of Reduced Nicotinamide Adenine Dinucleotide by Graphite Electrodes Modified with Adsorbed Aromatics Containing Catechol Functionalities. *Anal. Chem.* **1981**, *53*, 1979−1982.
(32) Remón, J.; Ochoa, E.; Foguet, C.; Pinilla, J. L.; Suelves, I. Towards a Sustainable Bio-Fuels Production from Lignocellulosic Bio-Oils: Influence of Operating Conditions on the Hydrodeoxygenation of Guaiacol over a Mo2C/CNF Catalyst. *Fuel Process. Technol.* **2019**, *191*, 111−120.
(33) Tohma, H.; Morioka, H.; Harayama, Y.; Hashizume, M.; Kita, Y. Novel and Efficient Synthesis of P-Quinones in Water via Oxidative Demethylation of Phenol Ethers Using Hypervalent iodine(III) Reagents. *Tetrahedron Lett.* **2001**, *42*, 6899−6902.
(34) Waghmode, S. B.; Mahale, G.; Patil, V. P.; Renalson, K.; Singh, D. Efficient Method for Demethylation of Aryl Methyl Ether Using Aliquat-336. *Synth. Commun.* **2013**, *43*, 3272−3280.
(35) Hoarau, C.; Pettus, T. R. R. Strategies for the Preparation of Differentially Protected Ortho-Prenylated Phenols. *Synlett* **2003**, 0127−0137.
(36) Machara, A.; Hudlický, T. Advances in N- and O-Demethylation of Opiates. *Targets Heterocycl. Syst.* **2016**, *20*, 113−138.
(37) Mirrington, R. N.; Feutrill, G. I. Orcinol Monomethyl Ether. *Org. Synth.* **1988**, *50*, 859.
(38) Nowakowska, M.; Herbinet, O.; Dufour, A.; Glaude, P. A. Kinetic Study of the Pyrolysis and Oxidation of Guaiacol. *J. Phys. Chem. A.* **2018**, *122*, 7894−7909.
(39) Ahmad, E.; Pant, K. K. Lignin Conversion: A Key to the Concept of Lignocellulosic Biomass-Based Integrated Biorefinery. *Waste Biorefinery* **2018**, *14*, 409−444.
(40) Zhang, H.; Wang, Y.; Shao, S.; Xiao, R. Catalytic Conversion of Lignin Pyrolysis Model Compound- Guaiacol and Its Kinetic Model Including Coke Formation. *Sci. Rep.* **2016**, *6*, 37513.
(41) Zhou, M.; Ye, J.; Liu, P.; Xu, J.; Jiang, J. Water-Assisted Selective Hydrodeoxygenation of Guaiacol to Cyclohexanol over Supported Ni and Co Bimetallic Catalysts. *ACS Sustainable Chem. Eng.* **2017**, *5*, 8824−8835.
(42) Xiao, F.; Yue, L.; Li, S.; Li, X. Conjugation of Cytochrome c with Ferrocene-Terminated Hyperbranched Polymer and Its Influence on Protein Structure, Conformation and Function. *Spectrochim. Acta, Part A* **2016**, *162*, 69−74.
(43) Ostojić, J.; Herenda, S.; Bešić, Z.; Miloš, M.; Galić, B. Advantages of an Electrochemical Method Compared to the Spectrophotometric Kinetic Study of Peroxidase Inhibition by Boroxine Derivative. *Molecules* **2017**, *22*, 1120.
(44) Petek, M.; Bruckenstein, S.; Feinberg, B.; Adams, R. N. Anodic Oxidation of Substituted Methoxyphenols. Mass Spectrometric

https://dx.doi.org/10.1021/acsomega.0c01846
ACS Omega 2020, 5, 16208−16219

Identification of Methanol Formed. *J. Electroanal. Chem. Interfacial Electrochem.* **1973**, *42*, 397−401.
(45) Shao, D.; Chu, W.; Li, X.; Yan, W.; Xu, H. Electrochemical Oxidation of Guaiacol to Increase Its Biodegradability or Just Remove COD in Terms of Anodes and Electrolytes. *RSC Adv.* **2016**, *6*, 4858−4866.
(46) Caballero, B.; Trugo, L. C.; Finglas, P. M. *Encyclopedia of Food Sciences and Nutrition*; 2nd Edition, Academic: 2003.
(47) Feng, P.; Wang, H.; Lin, H.; Zheng, Y. Selective Production of Guaiacol from Black Liquor: Effect of Solvents. *Carbon Resour. Convers.* **2019**, *2*, 1−12.
(48) Yang, X.; Zhang, F.; Hu, Y.; Chen, D.; Xiong, L. Gold Nanoparticals Doping Graphene Sheets Nanocomposites Sensitized Screen-Printed Carbon Electrode as a Disposable Platform for Voltammetric Determination of Guaiacol in Bamboo Juice. *Int. J. Electrochem. Sci.* **2014**, *9*, 5061−5072.
(49) Li, C.; Fu, J.; Tan, X.; Song, X.; Li, Q. A Simple and Effective Strategy Based on Sodium Gallate-Exfoliated Graphene for the Simultaneous Voltammetric Determination of Guaiacol and Vanillin. *Anal. Methods* **2019**, *11*, 4099−4105.
(50) Gan, T.; Shi, Z.; Deng, Y.; Sun, J.; Wang, H. Morphology-Dependent Electrochemical Sensing Properties of Manganese Dioxide-Graphene Oxide Hybrid for Guaiacol and Vanillin. *Electrochim. Acta* **2014**, *147*, 157−166.
(51) Sun, J.-y.; Gan, T.; Deng, Y.-p.; Shi, Z.-x.; Lv, Z. Pt Nanoparticles-Functionalized Hierarchically Porous γ-Al_2O_3 Hollow Spheres Based Electrochemical Sensor for Ultrasensitive Guaiacol Detection. *Sens. Actuators, B* **2015**, *211*, 339−345.
(52) Chawla, S.; Rawal, R.; Kumar, D.; Pundir, C. S. Amperometric Determination of Total Phenolic Content in Wine by Laccase Immobilized onto Silver Nanoparticles/zinc Oxide Nanoparticles Modified Gold Electrode. *Anal. Biochem.* **2012**, *430*, 16−23.
(53) Rawal, R.; Chawla, S.; Pundir, C. S. Polyphenol Biosensor Based on Laccase Immobilized onto Silver Nanoparticles/multiwalled Carbon Nanotube/polyaniline Gold Electrode. *Anal. Biochem.* **2011**, *419*, 196−204.
(54) Paxman, D. G.; Robinson, J. C. Regulation of Occupational Carcinogens under OSHA's Air Contaminants Standard. *Regul. Toxicol. Pharmacol.* **1990**, *12*, 296−308.
(55) Laviron, E. General Expression of the Linear Potential Sweep voltammogram in the Case of Diffusionless Electrochemical Systems. *J. Electroanal. Chem. Interfacial Electrochem.* **1979**, *101*, 19−28.
(56) Kumar, A. S.; Shanmugam, R.; Vishnu, N.; Pillai, K. C.; Kamaraj, S. Electrochemical Immobilization of Ellagic Acid Phytochemical on MWCNT Modified Glassy Carbon Electrode Surface and Its Efficient Hydrazine Electrocatalytic Activity in Neutral pH. *J. Electroanal. Chem.* **2016**, *782*, 215−224.
(57) Nagaoka, T.; Yoshino, T. Surface Properties of Electrochemically Pretreated Glassy Carbon. *Anal. Chem.* **1986**, *58*, 1037−1042.
(58) Putranto, R. P.; Mubarok, H.; Umam, K.; Saepudin, E.; Ivandini, T. A. Modification of Boron-Doped Diamond with Gold Nanoparticles and Its Preliminary Study for Electrosynthesis of Vanillin. *IOP Conf. Ser.: Mater. Sci. Eng.* **2019**, *496*, No. 012056.
(59) Scharf, U.; Grabner, E. W. Electrocatalytic oxidation of hydrazine at a Prussian blue-modified glassy carbon electrode. *Electrochim. Acta* **1996**, *41*, 233−239.
(60) Golabi, S. M.; Zare, H. R. Electrocatalytic oxidation of hydrazine at a chlorogenic acid (CGA) modified glassy carbon electrode. *J. Electroanal. Chem.* **1999**, *465*, 168−176.
(61) Zhu, J.; Chauhan, D. S.; Shan, D.; Wu, X.-Y.; Zhang, G.-Y.; Zhang, X.-J. Ultrasensitive determination of hydrazine using a glassy carbon electrode modified with pyrocatechol violet electrodeposited on single walled carbon nanotubes. *Microchim. Acta* **2014**, *181*, 813−820.
(62) Swetha, P.; Devi, K. S. S.; Kumar, A. S. In-situ trapping and confining of highly redox active quinolone quinones on MWCNT modified glassy carbon electrode and its selective electrocatalytic oxidation and sensing of hydrazine. *Electrochim. Acta* **2014**, *147*, 62−72.
(63) Patrice, F. T.; Qiu, K.; Zhao, L.-J.; Fodjo, E. K.; Li, D.-W.; Long, Y.-T. Individual modified carbon nanotube collision for electrocatalytic oxidation of hydrazine in aqueous solution. *ACS Appl. Nano Mater.* **2018**, *1*, 2069−2075.
(64) Sundaram, S.; Annamalai, S. K. Selective Immobilization of Hydroquinone on Carbon Nanotube Modified Electrode via Phenol Electro-Oxidation Method and Its Hydrazine Electro-Catalysis and Escherichia Coli Antibacterial Activity. *Electrochim. Acta* **2012**, *62*, 207−217.

https://dx.doi.org/10.1021/acsomega.0c01846
ACS Omega 2020, 5, 16208−16219